Expansion of the fetoplacental vasculature in late gestation is strain dependent in mice

Monique Y. Rennie, Jacqui Detmar, Kathie J. Whiteley, Andrea Jurisicova, S. Lee Adamson and John G. Sled

Am J Physiol Heart Circ Physiol 302:H1261-H1273, 2012. First published 20 January 2012; doi: 10.1152/ajpheart.00776.2011

Am J Physiol Heart Circ Physiol 302: H1261–H1273, 2012.
First published January 20, 2012; doi:10.1152/ajpheart.00776.2011.

Expansion of the fetoplacental vasculature in late gestation is strain dependent in mice

Monique Y. Rennie,[1,2,3] Jacqui Detmar,[3,4,6] Kathie J. Whiteley,[6] Andrea Jurisicova,[3,5,6] S. Lee Adamson,[3,5,6,*] and John G. Sled[1,2*]

[1]*Mouse Imaging Centre, Toronto Centre for Phenogenomics, Hospital for Sick Children, Toronto;* [2]*Department of Medical Biophysics,* [3]*Department of Obstetrics and Gynecology,* [4]*Institute of Medical Studies, and* [5]*Department of Physiology, University of Toronto, Toronto; and* [6]*Samuel Lunenfeld Research Institute, Mount Sinai Hospital, Toronto, Ontario, Canada*

Submitted 2 August 2011; accepted in final form 12 January 2012

Rennie MY, Detmar J, Whiteley KJ, Jurisicova A, Adamson SL, Sled JG. Expansion of the fetoplacental vasculature in late gestation is strain dependent in mice. *Am J Physiol Heart Circ Physiol* 302: H1261–H1273, 2012. First published January 20, 2012; doi:10.1152/ajpheart.00776.2011.— How the fetoplacental arterial tree grows and expands during late gestational development is largely unknown. In this study, we quantified changes in arterial branching in the fetal exchange region of the mouse placenta during late gestation, when capillarization increases rapidly. We studied two commonly used mouse strains, CD1 and C57Bl/6 (B6), at embryonic days (E)13.5, 15.5, and 17.5. B6 mice differ from CD1 mice by exhibiting a blunted fetal weight gain in late gestation. We found that B6 capillarization and interhemal membrane thinning were reduced and placental hypoxia-inducible factor-1α and VEGF-A expression were higher than CD1 near term. Automated vascular segmentation of microcomputed tomography data sets revealed that the number of arterial vessels ≥50 μm remained constant during late gestation in both strains, despite large increases in downstream capillary volume quantified by stereology (+65% in B6 mice and +200% in CD1 mice). Arterial diameters expanded in both strains from E13.5 to E15.5; however, diameters continued to expand to E17.5 in B6 mice only. The diameter scaling coefficient at branch sites was near optimal (−3.0) and remained constant in CD1 mice, whereas it decreased, becoming abnormal, in B6 mice at term (−3.5 ± 0.2). Based on arterial tree geometry, resistance remained constant throughout late gestation (~0.45 mmHg·s·μl^{-1}) in CD1 mice, whereas it decreased by 50% in late gestation in B6 mice. Quantification of the fetoplacental vasculature revealed significant strain-dependent differences in arterial and capillary expansion in late gestation. In both strains, enlargement of the fetoplacental arterial tree occurred primarily by increased arterial diameters with no change in segment numbers in late gestation.

microcomputed tomography; fetoplacental circulation; placenta; pregnancy; hemodynamics

A QUANTITATIVE DESCRIPTION of arterial vascular development is necessary for understanding vascular hemodynamics, the relationship between arterial vascular geometry and vascular function, and the consequences of insufficient vascularization on wall shear stress and vascular resistance. A network of finer and finer branched arterial vessels conduct blood toward the capillaries for the exchange of gases and nutrients. The bifurcating tree structure of the arterial vasculature has a large effect on the function of a vascular network. One of the challenges of assessing vascular morphology is the difficulty in obtaining accurate geometric data in a form that can be related to hemodynamic parameters. Recent advances in microcomputed tomography (micro-CT) imaging and computer analysis techniques have addressed this need and provide the automation needed to examine large numbers of specimens (52). Prior work on small numbers of specimens has provided detailed descriptions of arterial branching geometry in numerous adult organs, including the lung (61), kidney (44, 55), and liver vasculatures (34). However, these technological advances have not yet been exploited to study the development of a vascular tree in any organ.

In the present study, we examined the development of the fetoplacental arterial tree during late gestation. This tree delivers blood to an extensive and expanding capillary network with a large surface area for exchange and is vital for fetal growth and survival. Nevertheless, the factors that control normal late gestational growth and development of the fetoplacental vasculature are largely unknown. This dearth of knowledge is especially striking compared with the wealth of knowledge pertaining to the development of the nascent vasculature in the embryo (16) and of branching morphogenesis of lung bronchi (42) and renal tubules (8).

Much of our understanding of placental vascular development comes from studies on the mouse (2, 19). The mouse is a widely used model for studying placental development due to the relative ease of genetic manipulation (56), a placental vascular and cellular structure with similarity to that of the human (2, 18, 23), and the availability of inbred strains that provide genetically identical specimens for analysis.

The present study examined late gestational fetoplacental arterial vascular development in two of the most commonly used mouse strains in placental research (e.g., Refs. 2, 12–14, 17, and 43). CD1 mice are an outbred strain often used to study normal pregnancy and fetal development. C57Bl/6 (B6) mice are the most commonly used inbred strain, and they are often used as the background strain for transgenic and knockout mouse models. We focused on late gestational fetoplacental arterial development from embryonic day (E)13.5 to E17.5. At E13.5, the placenta undergoes a remarkable molecular transition when ~4,000 genes suddenly alter their expression by >1.5-fold (35). This marks a transition from the "development phase" during organogenesis to the "mature phase" of late gestation (35). After E13.5, B6 capillary length increases by ~10-fold (14). How the arterial tree grows and expands to supply this expanding capillary bed in late gestation is unknown.

In the present study, we exploited advances in micro-CT imaging and computer analysis to quantify the geometry and branching pattern of the developing fetoplacental arterial tree in CD1 and B6 mice. These data were used to predict the

* S. L. Adamson and J. G. Sled contributed equally to this work.
Address for reprint requests and other correspondence: S. L. Adamson, Samuel Lunenfeld Research Institute, Mount Sinai Hospital, 60 Murray St., Box 42, Toronto, ON, Canada M5T 3H7 (e-mail: adamson@lunenfeld.ca).

influence of geometric changes on fetoplacental arterial vascular resistance and shear stress, and stereological techniques were used to assess capillary growth in both strains.

METHODS

Mice. Experimental procedures were approved by the Animal Care Committee of Mount Sinai Hospital and the Toronto Centre for Phenogenomics and were conducted in accordance with guidelines established by the Canadian Council on Animal Care. CD1 and B6 mice were purchased from Charles River Laboratories (Montreal, QC, Canada). Males were mated in house with virgin females aged 10–12 wk. The morning that a vaginal copulation plug was detected was designated E0.5.

Injection of contrast agent and CT scanning. Methods for the injection of the radioopaque silicone rubber X-ray contrast agent (Microfil, Flow Tech, Carver, MA) into the fetoplacental vasculature for micro-CT imaging have previously been described (53, 60). In brief, blood was cleared from the fetoplacental vasculature of surgically exposed fetuses by perfusing heparinized saline with added xylocaine (for vasodilation) via the umbilical circulation (60). Contrast agent was then infused gently by hand via the single umbilical artery until its bright yellow color could be seen in the capillary bed. At this point, the vessels were tied off to maintain pressure during polymerization of the silicone rubber. After polymerization, the umbilical cord was severed, and the placenta was immersed in fixative (10% buffered formalin phosphate) for 24–48 h at 4°C. Vasculatures with visibly incomplete filling or vessel inflation were excluded before imaging as described in our prior work (53). Specimens were mounted in 1% agar gel made with 10% formalin in preparation for scanning. Seven to ten specimens were obtained per group. There were at least four dams per group with one to three specimens obtained from each litter. Umbilical artery diameters measured by micro-CT have been previously shown to differ from in vivo microultrasound measurements by <5% (53).

In separate animals, the arterial fetoplacental vasculature was perfused with methyl methacrylate casting compound (Batson's no. 17, Polysciences, Warrington, PA) and processed for scanning electron microscopy (SEM) using established methods (60). These specimens were viewed using a PEI XL30 scanning electron microscope (FEI Systems Canada, Toronto, ON, Canada).

Three-dimensional data sets of Microfil-perfused specimens were acquired using an MS-9 micro-CT scanner (GE Medical Systems, London, ON, Canada) as previously described (52, 53). Each specimen was rotated 360° around the vertical axis, generating 720 views that were subsequently reconstructed into data blocks with a 13-μm voxel size. Vascular surface renderings were generated from micro-CT data to visualize the arterial vasculature as previously described (53). Umbilical artery diameters and fetoplacental arterial span and depth were measured directly from these surface renderings via digital calipers using the Amira software package (Visage Imaging, San Diego, CA).

Vascular segmentation and hemodynamic modeling. The vascular segmentation of fetoplacental micro-CT datasets has been previously described in detail (52). Vessel segments and bifurcations were identified automatically by a segmentation algorithm. The algorithm returned the center lines of a connected vessel tree and a tubular model in which the lengths, diameters, and connectivity of each vessel segment were known. Measurements of vascular length, vessel segment numbers, diameter scaling coefficient (for all vessels >100 μm), and the distributions of vessel diameters and vascular volumes were extracted from the resultant tubular models. We (52) have previously shown that automated vascular segmentation is highly accurate (diameters within 3%) and reproducible (coefficient of variation <3%) for fetoplacental vessels >50 μm in diameter. SEM imaging of the E15.5 arterial-only perfused fetoplacental tree revealed that the arteriole vessels that lead into capillary tufts typically have diameters >50 μm at E15.5, as shown in Fig. 1. Therefore, this threshold for automated vascular segmentation is appropriate for identifying the majority of arterial vessels in the fetoplacental tree.

Growth of the fetoplacental tree with increasing gestation was estimated from cross-sectional data in both strains. Assuming that as a placenta grows the order of its vessels remains constant (e.g., the largest vessel remains the largest vessel), growth between two ages can be estimated. Growth modeling analysis was performed to determine which vessels of the tree were enlarging from one gestational age to the next and to evaluate whether enlargement patterns differed between strains. Two difficulties arose when estimating the growth of a group of placentas from one time point to another: *1*) the total number of segments making up a fetoplacental tree differed within a group for a given gestation and *2*) the mean number of segments differed between gestations. To deal with the first issue, the mean number of segments, *n*, was computed for all the placentas of a given group. The ordinal numbering of vessel segments was remapped so that the largest vessel was ordered 1 and the smallest was ordered *n*, where *n* is the mean number of vessel segments in that group. These

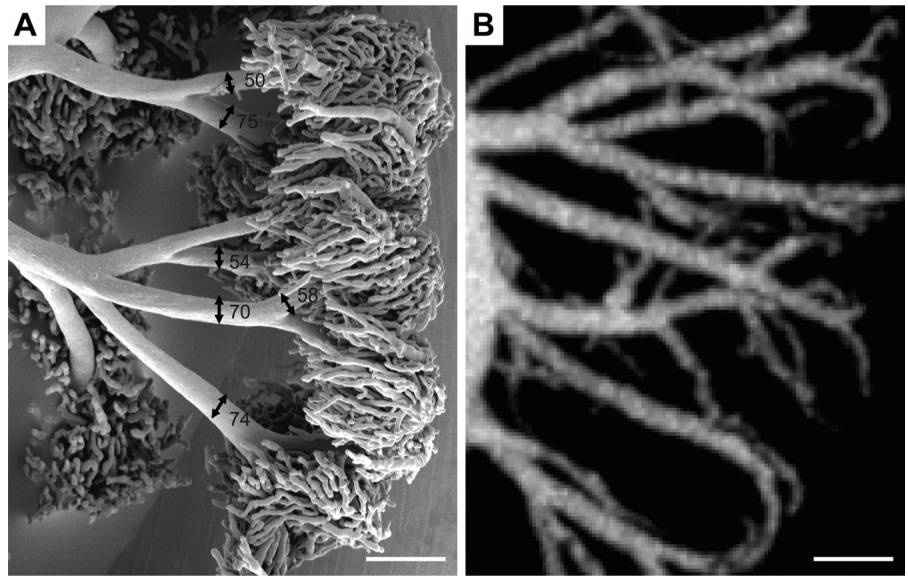

Fig. 1. Vessel diameters at the arteriole to capillary transition zone. *A*: scanning electron microscopy image of an embryonic day (E)13.5 CD1 placenta selectively perfused to fill only the arterial vessels and the transition into capillaries. Vessel diameters are shown in micrometers. The arteriole vessels that branch into capillary tufts in this representative image range from 50 to 75 μm in diameter. *B*: maximum intensity projection image of an E13.5 CD1 placenta imaged with microcomputed tomography. Scale bars in *A* and *B* = 200 μm.

data were then interpolated so as to have a list of exactly n diameters for each placenta from which a group mean diameter at each order, 1 through n, could be computed. To deal with the second issue, if one group had more vessels than the other, the growth transformation was computed for only the first m largest vessels, where m was the lesser of the mean number of vessels in the two groups. Once the relationship between diameters in the two groups was established, the percent difference between corresponding vessels in the earlier and later time point was computed.

The resistance through the arterial network was calculated based on vessel geometry through use of standard formulas for resistances in parallel and in series as previously described (61). Hemodynamic calculations assumed *1*) Poiseuille's law for flow of fluid through a pipe-like structure, *2*) equal pressure at each terminal vessel, and *3*) a correction factor modeling blood viscosity changes in small vessels derived using adult blood (49). In vivo umbilical artery blood flow (Q) was estimated using the following equation: $Q = \pi(d/2)^2 v$, where d is the umbilical artery diameter measured from our micro-CT data and v is the time-averaged mean blood velocity. These diameter measurements have been previously validated against in vivo measurements obtained with microultrasound (53). Average umbilical artery velocity over the cardiac cycle was estimated from peak systolic velocity profiles from the literature (37, 43) by assuming a parabolic blood velocity profile (mean velocity = 0.5 × peak velocity) and an average velocity over the cardiac cycle corresponding to half the peak velocity, as previously described (52). We used the estimated flow together with our calculated resistance measurements to calculate the pressure differential between the umbilical artery and the smallest vessels included in our study (50 μm) for each data set. Wall shear was computed for each vessel using the following formula: shear = $32Qv/\pi d^3$, where v is blood viscosity.

The mean umbilical artery pressure drop was estimated by assuming mean aortic pressure is ~50% peak systolic pressure measured in the heart of mouse embryos (29) at E13.4 and E14.5 and then taking a linear extrapolation to mean carotid arterial pressure measured at postnatal *day 1.5* in mouse pups (28). Estimations also assumed mean arterial pressure at the placenta is ~60% of the value of central arterial pressure based on measurements of pressures in near-term fetal sheep (3).

Stereology. One or two placentas per litter from three CD1 dams and three B6 dams at both E15.5 and E17.5 were processed for stereology (n = 5–6 placentas per group per gestational age) using established methodologies (14). Formalin-fixed placentas were mounted and sectioned on a vibratome (VT1200, Leica) from a random starting point into 0.7-mm-thick systematic random sections perpendicular to the chorionic plate. The four to nine sections obtained per placenta were mounted into a single block. Two 5-μm sections were cut from each block. The first was stained with hematoxylin and eosin using standard protocols to estimate the volumes of placental zones. The second was stained with anti-CD34 as outlined below to quantify fetal blood space, maternal blood space, and interhemal membrane thickness. Stereological analysis was performed using light microscopy and the New Computer Assisted Stereology Toolbox (NEWCAST) system from Visiopharm (Hoersholm, Denmark).

Placental volume and volume densities were estimated using the point counting method as previously described (14, 27). Volume densities were converted to absolute component volumes by multiplying by the total volume of the placenta. Interhemal membrance thickness was measured using the orthogonal intercept method (31). Harmonic mean thickness required a correction factor of $(8/3)\pi$ to correct for the plane of sectioning (9). All volumes and thicknesses were corrected for shrinkage, as assessed by comparing the diameter of maternal erythrocytes on slides with diameter measurements obtained from fresh maternal erythrocytes, as previously described (14).

Methods for Western blot analysis and immunohistochemistry. Three placentas were bisected, and half of each placenta was pooled per litter from four CD1 dams and four B6 dams at E13.5, E15.5, and E17.5. Placental tissue was used to assess protein expression by Western blot analysis (n = 4 dams per group per gestational age). Blots were probed with anti-hypoxia-inducible factor (HIF)-1α (1:500, NB100-134, Novus Biologicals, Littleton, CO) or anti-VEGF (1:100, sc-507, Santa Cruz Biotechnology, Santa Cruz, CA) antibodies using standard methods as previously described (21). Blots were stripped and reprobed with anti-β-actin antibody (1:400, sc-1,616, Santa Cruz Biotechnology) to control for protein loading. One to two placentas per litter from three CD1 dams and three B6 dams at E15.5 and E17.5 were embedded in paraffin and probed with anti-HIF-1α antibody (Novus Biologicals) diluted 1:200 as previously described (21) or with CD34 using rat anti-mouse CD34 antibody (Serotec) diluted 1:100. Densitometric analyses were done using ImageQuant software.

Statistical analysis. Three-factor ANOVA was used to assess variance due to litter, gestational age, and strain. Litter was a significant factor in fetal and placental weights so litter means were used for statistical analysis. Litter was not a significant factor for vascular data obtained via micro-CT or stereology so individual placentas were used as the experimental unit in two-way ANOVA to evaluate effects of strain and gestational age. To determine statistical significance in the growth modeling data, the growth curves were subdivided by vessel size and three-way ANOVA was performed to evaluate the effects of vessel type, strain, and gestational age (E13.5 to E15.5 or E15.5 to E17.5). If the ANOVA was significant, Tukey post hoc tests were performed. All statistical tests were performed using R statistical software (www.r-project.org). P values of <0.05 were considered significant.

RESULTS

CD1 mice are an outbred strain and are prolific breeders. They had litter sizes that were approximately double those of B6 mice (Fig. 2*A*). Fecundity in our B6 animals (~6–7 fetuses/litter) was similar to prior reports and other inbred strains (http://phenome.jax.org). Placental weights were similar in the two strains and did not significantly change with gestation (Fig. 2*C*). Both strains also had similar fetal body weights and a similar near twofold increase in fetal body weight between E13.5 and 15.5 (Fig. 2*B*). Fetal body weight continued to increase to E17.5 in both strains, but this increase was blunted in B6 fetuses such that B6 fetuses weighed ~20% less than CD1 fetuses at E17.5 (Fig. 2*B*). In the placenta, HIF-1α and VEGF-A protein levels were similar between strains at E13.5 (Fig. 3). Levels did not increase significantly with age in CD1 mice. In contrast, in B6 mice, placental VEGF-A protein levels increased approximately fourfold at E15.5 and placental HIF-1α increased almost twofold at E17.5 (Fig. 3*B*). Thus, reduced late gestational fetal growth in B6 pregnancies was associated with elevations in placental proteins known to be upregulated in response to hypoxia. This suggests that B6 fetal growth may be limited by less effective placental function. Therefore, we used micro-CT and stereological analysis in both strains to evaluate the morphological changes associated with expansion of labyrinthine vasculature in late gestation.

Stereological measurements at E15.5 and E17.5 showed no differences in volumes of the whole placenta or of its components (labyrinth, junctional zone, decidua, or chorionic plate) between the two strains at either age studied (Table 1). Only the labyrinth increased in volume over this age range (by ~60–80%). Of the labyrinth volume, fetal capillary volume occupied ~15–19% at E15.5 in both strains (Table 2). Maternal blood space in the labyrinth occupied ~25–27%, and this proportion did not change with age, nor did it differ between the two strains. Whereas the increase in fetal capillary volume at E17.5 in B6 mice merely kept pace with the increase in

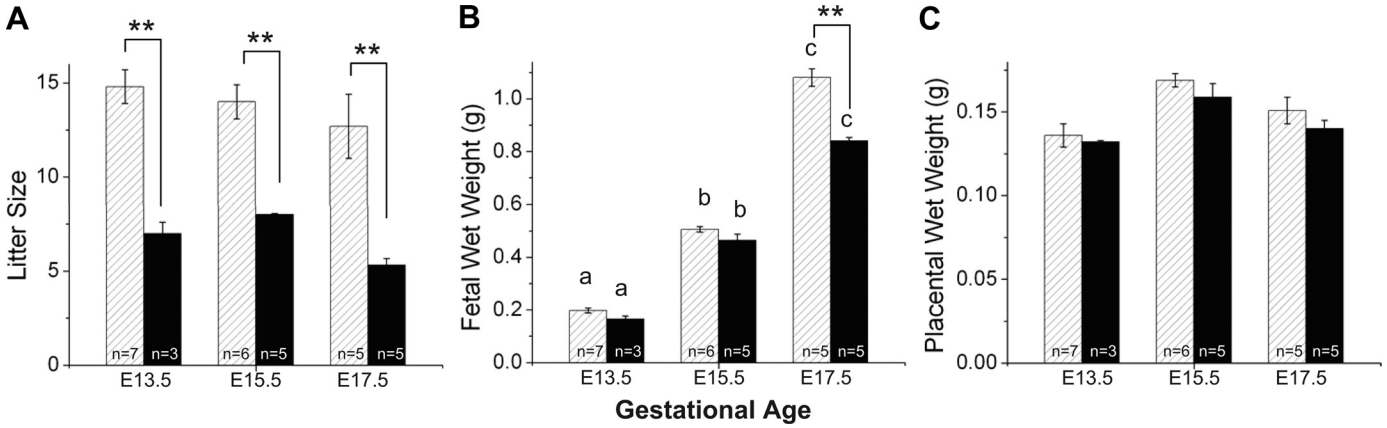

Fig. 2. Developmental changes in CD1 (hatched bars) and C57B1/6 (B6; solid bars) mice during late gestation. Litter sizes (*A*), fetal weights (*B*), and placental weights (*C*) are shown as means ± SE. ANOVA showed that litter was a significant source of variation in fetal and placental weights, so in these graphs *n* refers to the number of dams. [a,b,c]Differences with gestational age; $^{**}P < 0.001$, strain differences.

labyrinth volume, CD1 mice showed a much larger increase in fetal capillaries such that they occupied ~26% of the labyrinth volume by E17.5 (Table 2). Interestingly, at E17.5, fetal capillary volume in CD1 mice had increased to become equal to maternal blood space volume (Fig. 4, *A* and *B*), which we speculate may be optimal for maternofetal transfer. The diffusional barrier to maternal-fetal exchange, the interhemal membrane, thinned with advancing gestation in both strains (Fig. 4*C*). However, it was significantly thicker at both ages in B6 placentas compared with CD1 placentas. As this would be anticipated to impede maternofetal exchange, it is possible that impaired exchange induced the higher VEGF protein levels observed in B6 placentas at E15.5. These results suggested that the reduced growth rate of fetuses in B6 pregnancies between E15.5 and E17.5 may be caused by a blunted rise in capillarization of the labyrinth in late gestation as well as by a larger interhemal thickness. Therefore, the placenta may be less effective as a gas exchanger, possibly explaining the higher placental VEGF and HIF-1α protein levels in late gestation in this strain (Fig. 3).

We next examined the fetoplacental arterial vasculature that supplies the capillaries of the labyrinth. We visualized the arterial tree at E13.5, E15.5, and E17.5 using three-dimensional vascular surface renderings generated from micro-CT data. Images showed that in both strains a centrally located umbilical artery branched across the chorionic plate before branching into smaller diameter intraplacental arteries (Fig. 5). The arterial trees became more elaborate with advancing gestation, but changes with age were not striking, nor were there immediately obvious differences between the two strains. This was surprising given the estimated 2- to 3.5-fold increase in blood flow through this tree over this age range in both CD1 and B6 mice (Table 3). Individual variations in branching pattern may make significant differences difficult to detect by visual examination alone. Therefore, to quantitatively evaluate these detailed branching structures, we used automated segmentation methods. Prior work (52) has shown that vessels as small as 50 μm can be reliably segmented and analyzed. Batson's corrosion casts were used to identify vessels in this caliber range in the fetoplacental vascular tree. The results showed that the vast majority of vessels in the fetoplacental arterial tree exceeded this threshold (Fig. 1). Only capillaries and some of the smallest vessels leading directly into capillaries were excluded. The results also indicated that arteriole vessels, which are generally thought to be the site of highest resistance in the tree, ranged from 50 to 75 μm in diameter in the fetoplacental tree; thus, these vessels were included in our analysis.

Geometry of CD1 and B6 arterial trees. In both strains, quantification revealed that from E13.5 to E17.5 there was a significant increase in the depth of the tree (by ~45%) and the total volume of all vessels in the tree (~60%), whereas the span of the tree did not change significantly with gestation (Table 4). However, there was no significant change in the total number of vessel segments in the tree and only a small increase in their total length (~20%; Table 4). Additionally, no significant change in the length of vessel segments for any given diameter (i.e., the length-to-diameter ratio) was observed. Indeed, the only parameter that differed between the two strains was the diameter scaling coefficient; whereas this did not change with age in CD1 placentas (approximately −2.9), the diameter scaling coefficient of B6 placentas (approximately −3.0) decreased significantly at E17.5 to −3.5 (Table 4). This change indicated that at E17.5, diameters decreased more slowly with successive branching in B6 mice compared with CD1 mice. Furthermore, the diameter scaling coefficient for B6 placentas became abnormal relative to values reported in arterial trees of other organs (32, 34, 44, 45).

Further examination of the growth of the tree as a function of vessel diameter revealed additional differences between the strains. When the cumulative number of vessel segments was plotted as a function of diameter, a significant rightward shift between the E13.5 and E15.5 curves of both strains was observed primarily in the mid diameter range (~100–150 μm; Fig. 6, *A* and *B*). Since the total number of vessel segments remained constant, we interpret this as showing that vessels in this size range tend to increase in diameter over this interval. However, whereas intraplacental artery growth continued between E15.5 and E17.5 in B6 placentas (i.e., a further rightward shift), there was no further growth in CD1 placentas (Fig. 6*A*). This was also observed as a progressive increase in the number and total length of segments in this diameter range in B6 placentas, whereas CD1 placentas increased between E13.5 and E15.5 and then remained constant until E17.5 (Fig. 6, *C–F*). These results indicated that the way in which the arterial tree grew with gestation differed between the two strains.

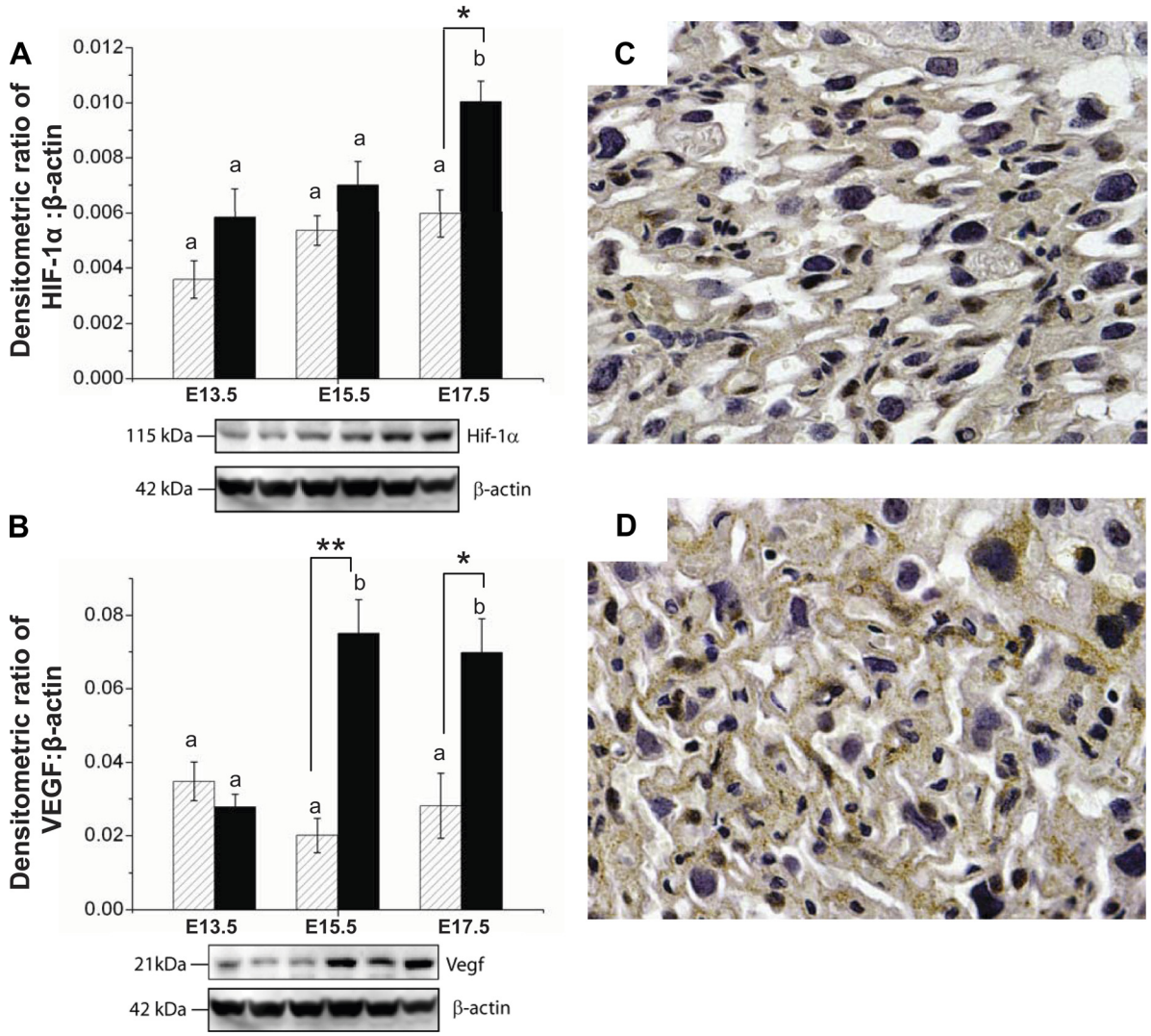

Fig. 3. Potential factors driving vascular development in CD1 (hatched bars) and B6 (solid bars) mice. Western blots showed increased expression of hypoxia-inducible factor (HIF)-1α protein (*A*) in B6 placentas at E17.5 and VEGF protein (*B*) in B6 placentas at E15.5 and E17.5. The order of the lanes corresponds to the order of the bars on the graph. *C* and *D*: representative images of the CD1 (*C*) and B6 (*D*) placental labyrinth at E17.5 immunostained for HIF-1α. Sections from one placenta per litter from three CD1 dams and three B6 dams were examined. Staining in B6 mice was more pronounced. Western blot data are presented as means ± SE, where $n = 4$ dams per group per gestational age (tissue pooled from 3 placentas/litter). Two-way ANOVA was used to assess the effects of gestational age and strain. [a,b]Differences with gestational age; $*P < 0.05$ and $**P < 0.001$, strain differences as determined by Tukey post hoc tests.

We next quantified enlargement of diameters in the arterial tree using growth modeling analysis. We determined the percent change in diameter versus age as a function of vessel diameter in the two strains. In both strains, between E13.5 and E15.5, percent enlargement was generally 2–10% (Fig. 7). However, between E15.5 and E17.5, there was little enlargement at most diameters in CD1 arterial trees, whereas 75- to 150-μm intraplacental arteries continued to expand in B6 placentas (Fig. 7). In contrast, over this age range, vessels in the size range characteristic of the chorionic plate (>200 μm) appeared to expand very little in both strains (Fig. 7).

Table 1. *Absolute volumes of placental components in CD1 and B6 placentas at two stages of late gestation*

	CD1 Mice		B6 Mice	
	E15.5	E17.5	E15.5	E17.5
No. of placentas/group	5	6	6	5
Placenta	90.7 ± 10.1	112.4 ± 6.4	89.7 ± 10.3	91.8 ± 6.6
Labyrinth Zone	30.3 ± 3.4[a]	56.3 ± 2.1[b]	26.8 ± 2.1[a]	42.5 ± 5.9[b]
Junctional Zone	30.6 ± 4.2	25.6 ± 3.0	32.9 ± 4.9	24.2 ± 4.9
Decidua Basalis	21.1 ± 3.4	20.0 ± 2.4	24.3 ± 4.0	18.4 ± 1.5
Chorionic Plate	7.9 ± 1.5	9.1 ± 1.5	5.5 ± 1.8	6.6 ± 1.6

Data are means ± SE (in mm^3). B6, C57B1/6; E, embryonic day. [a,b]Different letters show a significant difference between gestational ages ($P < 0.05$) as determined by two-way ANOVA followed by Tukey post hoc tests. Significant differences in absolute volumes were not detected between strains by two-way ANOVA.

Table 2. *Labyrinthine proportions of B6 and CD1 placentas*

	CD1 Mice		B6 Mice	
	E15.5	E17.5	E15.5	E17.5
No. of placentas/group	5	6	6	5
Fetal capillaries	15.6 ± 0.6[a]	25.7 ± 1.5[b]	19.4 ± 1.9	20.0 ± 1.1*
Maternal blood space	26.6 ± 3.0	25.8 ± 1.1	24.9 ± 2.2	26.8 ± 2.5
Other	57.9 ± 2.8[a]	48.5 ± 1.9[b]	55.7 ± 2.2	53.1 ± 2.0

Data are means ± SE (in %). [a,b]Different letters show a significant difference between gestational ages ($P < 0.05$); *$P < 0.05$, significant difference between strains at the same gestational age as determined by two-way ANOVA followed by Tukey post hoc tests.

Hemodynamic predictions based on network geometry of arterial trees. We next determined whether these interstrain differences in arterial vascular growth would be predicted to alter hemodynamic function. We calculated vascular resistance based on the network geometry of the tree. The results showed that the calculated vascular resistance of the fetoplacental arterial tree decreased significantly between E13.5 and E15.5 in both strains (by ~22%). Whereas resistance then stabilized in CD1 mice, resistance continued to decrease by 38% to E17.5 in B6 mice (Table 3). This result is consistent with the continued expansion of the arterial tree in late gestation, which occurred in B6 placentas only. We then used literature values for umbilical artery blood velocities and our measured umbilical artery diameters to estimate fetoplacental blood flow. These results indicated that there was a progressive increase in blood flow with gestational age in both strains (Table 3). Based on these blood flows, the wall shear stress as a function of vessel diameter was calculated at each age for each strain. At younger gestations, these calculations suggested that the shear stress distributions were comparable in the two strains, increasing similarly from E13.5 to 15.5 (Fig. 8). However, shear stress continued to rise in late gestation in CD1 placentas only. These results indicate that endothelial cells in CD1 and B6 arterial trees are exposed to different levels of shear stress, which may alter endothelial cell function.

Fetoplacental blood flow depends on the total resistance of the umbilicoplacental circulation (including the umbilical vessels, the arterial and venous vascular trees, and the capillaries) and the aorta to vena cava blood pressure gradient. To estimate the proportion of vascular resistance localized to the arterial tree, we estimated the pressure drop across the tree using our calculated values for resistance and fetoplacental blood flows. Our data predicted that the pressure drop across the arterial tree was 1–2 mmHg at E13.5 and E15.5 in both strains (Table 3). At E17.5, whereas the pressure drop increased to ~3 mmHg in CD1 mice due to the increase in flow and no change in resistance, no such increase in pressure drop was predicted to occur in B6 mice. Based on estimates of fetoplacental blood flow and umbilical artery pressure versus age, the proportion of total umbilicoplacental vascular resistance associated with the arterial tree would be ~30% at all ages for CD1 mice and for B6 mice at E13.5 and E15.5. This decreases to ~10% in B6 mice at E17.5 (Table 3). These results suggest that the arteriolar level of the circulation does not dominate fetoplacental vascular resistance; resistance in the capillaries and venous outflow tract is generally greater than that of the arterial tree. The results also showed that the arterial tree in B6 mice decreases its resistance in late gestation and therefore would not be a factor limiting fetoplacental perfusion of capillaries, and hence exchange, in late gestation in this strain.

DISCUSSION

The present study is the first to use micro-CT, vascular segmentation, and computational flow modeling to quantitatively evaluate morphological and functional changes with development of the fetoplacental arterial tree. To our knowledge, this study is also the first to use these techniques to study the development of a vascular tree in any organ of any species. Over late gestation, the number of arterial vessels in the

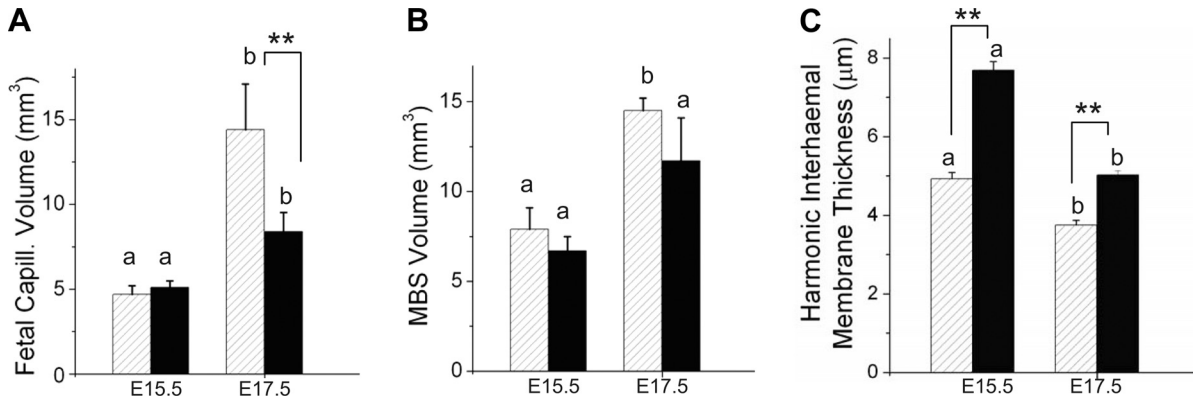

Fig. 4. Components of the labyrinth zone in CD1 (hatched bars) and B6 (solid bars) mice as assessed by stereology. The total labyrinthine volume is composed of fetal capillaries (*A*), maternal blood spaces [maternal blood space (MBS) volume; *B*], and other tissues that separate the two vascular systems (not shown). The interhemal barrier (*C*) separates maternal and fetal blood. Data are shown as means ± SE; *n* is the number of placentas. One or two placentas per litter from three CD1 dams and three B6 dams at E15.5 and E17.5 were processed for stereology (n = 5–6 placentas per group per gestational age). [a,b,c]Gestational age differences; **$P < 0.001$, strain differences determined using ANOVA followed by Tukey post hoc tests.

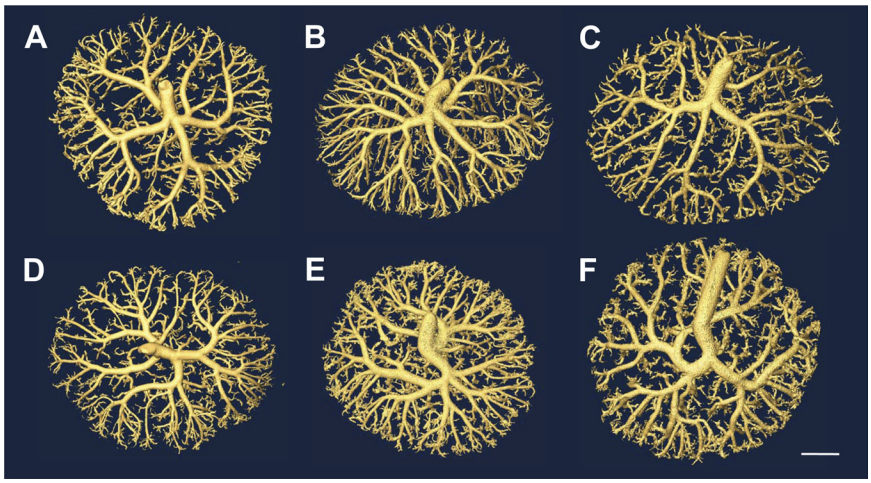

Fig. 5. Isointensity surface renderings of fetoplacental arterial vascular trees from CD1 (*A–C*) and B6 (*D–F*) mice from three gestational ages: E13.5 (*A* and *D*), E15.5 (*B* and *E*), and E17.5 (*C* and *F*). Scale bar = 1 mm.

placenta surprisingly remained constant despite a large increase in the volume of capillaries supplied by those vessels. CD1 and B6 arterial trees developed similarly from E13.5 to E15.5; however, novel growth modeling software revealed the continued expansion of vessel diameters from E15.5 to term in B6 mice only. Additionally, both interhemal membrane thinning and capillarization were blunted in B6 mice relative to CD1 mice, which may contribute to the blunted fetal growth observed in the B6 strain at term. In CD1 trees, resistance was predicted to stay constant throughout late gestation, whereas changes in B6 vascular geometry led to significant decreases in arterial vascular resistance. In CD1 trees, shear stress rose incrementally over late gestation, whereas shear stress decreased significantly in B6 mice from E15.5 to term. Elaboration of the CD1 tree appeared similar to normal human placental development, while the blunted capillarization and reduced rate of fetal growth observed in B6 mice appeared similar to pathologies observed in human intrauterine growth restriction (IUGR) (36, 39).

Fetoplacental arterial patterning. Prior work has suggested a strong genetic component to the development of the umbilical artery and the initial branching pattern of the villous tree. Coordinated expression of receptors and ligands on the chorioallantoic surfaces mediates central attachment of the allantois on the chorion (19). The umbilical artery forms between E8.5 and E9.5 of gestation by vasculogenesis within the allantois, before the onset of fetal blood flow (43), suggesting that the umbilical artery's central location and vasculogenesis are dependent on genetics more than flow or local factors. At E8.5, clusters of glial cells missing homolog 1 (Gcm1) expression in the chorion define where primary villi will form and become vascularized (4), establishing a basic pattern for arterial penetration into the labyrinth from the chorionic plate. Our data show that chorionic plate arteries by E13.5 are generally larger than ~200 μm (52); thus, arterial vessels penetrating the labyrinth would be ~100–200 μm in diameter. Approximately 200 sites of Gcm-1 expression (4) lead to 105–129 vessels of this size range in CD1 mice. Together, this suggests a strong genetic component to the initial branching pattern of the villous tree; however, the roles of genes, local physical and metabolic factors, and maternal versus fetal factors in the development of the remaining arteries and arterioles are not well understood.

Finer branching of arterial trees is thought to follow from patterning rules rather than having each branch location, diameter, and length genetically determined (41). This would mean that for the >1,100 intraplacental arteries and arterioles the geometry of each generation of branching is similar to the generation above, yielding a tree that is self-similar (24). Genetic determination of patterning rules that dictate branching pattern has been well established in kidney tubules (8) and pulmonary airways (40). The length-to-diameter ratios and diameter scaling coefficients measured in the present study suggest that patterning rules also apply to the fetoplacental arterial tree. The range of length-to-diameter ratios observed (2.3–2.8) was very similar to that of the adult mouse lung (2.3–2.6) (61), suggesting that branching pattern similarities may also extend to arterial trees in different tissues and at different developmental stages. A diameter scaling coefficient of approximately −3 was observed throughout development in CD1 placentas. This is in accord with Murray's law for the optimal arrangement of vessels, which predicts that a coefficient of −3 will maximize flow while minimizing biological work (54). This is also similar to reports of −3 and −2.97 from other adult arterial trees in rodents (kidney and liver) determined using similar techniques (34, 44). A decrease in the diameter scaling coefficient from −3 to −3.5 was observed in B6 placentas at E17.5, suggesting that diameters decreased more slowly across branching generations at this time point in B6 mice compared with CD1 mice. The E17.5 value in B6 mice is a departure from Murray's law and is outside the range of diameter scaling values reported in the literature (−2.7 to −3.0) (32, 34, 44, 61), implying that the intraplacental artery branching pattern in B6 mice is abnormal. A strain difference in the diameter scaling coefficient supports the idea that genes contribute significantly to the specification of arterial patterning rules. Nevertheless, the strong overall similarity of fetoplacental arterial branching to arterial branching in other organs suggests that patterning rules may be specified by the same genetic program and thus apply to the development of arterial trees in general.

The transition from arterioles to capillaries appears to be very abrupt in the mouse placenta. SEM images revealed that arterioles (50–75 μm in diameter) branch almost directly into capillaries [~11 μm (14)], suggesting that if there are arteriole vessels in the 10- to 50-μm diameter range they must be very short and few in number. Although micro-CT can image fetoplacental vessels down to ~30 μm in diameter (53), we (52) have previously shown an inflection point at 50 μm on cumulative diameter

Table 3. *Hemodynamics across the mouse fetoplacental tree*

	Associated Variables/Calculations	CD1 Mice			B6 Mice		
		E13.5	E15.5	E17.5	E13.5	E15.5	E17.5
Mean umbilical artery pressure drop (estimated), mmHg†	P	3	6	11	3	6	11
Mean umbilical artery blood velocity (estimated; V_{mean}), mm/s†	V_{mean}	25	25	31	30	30	34
Umbilical artery diameter from micro-CT data, mm	d	0.32 ± 0.02[a]	0.46 ± 0.01[b]	0.54 ± 0.01[c]	0.39 ± 0.02[a,*]	0.51 ± 0.02[b]	0.50 ± 0.01[b]
Umbilical artery flow (calculated), mm^3/s	$Q = V_{mean}[\pi(d/2)^2]$	2.0	4.1	7.1	3.6	6.1	6.8
Pressure drop across the arterial tree, mmHg	$P_{arterial}$	1.06 ± 0.09[a]	1.69 ± 0.19[a]	2.97 ± 0.50[b]	1.42 ± 0.13[a]	1.85 ± 0.10[b]	1.28 ± 0.12[b,**]
Fetal placental resistance, $mmHg \cdot s \cdot \mu l^{-1}$	$R_{total} = P/Q$	1.5	1.5	1.5	0.8	1.0	1.6
Resistance from micro-CT data, $mmHg \cdot s \cdot \mu l^{-1}$	$R_{arterial}$	0.52 ± 0.04[a]	0.41 ± 0.05[b]	0.42 ± 0.07[b]	0.39 ± 0.04[a]	0.30 ± 0.02[b]	0.19 ± 0.02[c,**]
Capillary and venous resistance, $mmHg \cdot s \cdot \mu l^{-1}$	$R_{cap+veins} = R_{total} - R_{arterial}$	1.0	1.1	1.1	0.4	0.7	1.4

Data are means ± SE; n = 7-10 placentas/group. micro-CT, microcomputed tomography. †Estimated from the literature. [a,b,c]Different letters show a significant difference between gestational ages ($P < 0.05$); *$P < 0.05$ and **$P < 0.001$, significant differences between strains at the same gestational age as determined by two-way ANOVA followed by Tukey post hoc tests. No statistical tests were performed on estimated values or calculated values that involved estimates.

distribution curves, below which the slopes of the curves were noticeably decreased. We inferred that this was an artifact and that vessels <50 μm could not be reliably segmented. However, the SEM images from the present study suggest that the segmentation may indeed be reliable for smaller diameter vessels and that the majority of vessels larger than capillaries in the fetoplacental tree are visible by micro-CT.

Growth of the fetomaternal microcirculation. Capillaries and maternal blood spaces of the labyrinth were quantified using stereology. Fetal blood in capillaries is separated from maternal blood by an interhemal membrane, which thins as gestation advances (12, 14), thereby reducing the barrier to maternofetal exchange. At term, membrane thickness was 34% greater in B6 mice compared with CD1 mice, suggesting a greater impediment to exchange. An additional exchange deficiency in B6 placentas would be anticipated due to their much reduced fetal blood space volume, which is 60% lower than that of CD1 placentas at term. Previous studies (12, 15) have shown that fetal blood space volume is less than maternal blood space volume earlier in gestation but increases to become approximately equal at term. While we observed this in CD1 mice, in B6 mice fetal blood space volume was ~30% less than maternal blood space volume at term. This leads us to speculate that B6 fetal blood space expansion does not take full advantage of the available maternal blood space volume and that this possibly contributes to the relatively poor growth rate in B6 embryos in late gestation. Fetal blood space volume is also less than maternal blood space volume at term in Balb/C mice, another inbred strain (57). Balb/C birth weights are similar to B6 birth weights (~0.90 g), and Balb/C fecundity (~7 pups/litter) (57) is similar to other inbred strains (http://phenome.jax.org). The similar placental vascularity in B6 and Balb/C strains suggests the reduced fecundity in inbred strains may, at least in part, be caused by reduced fetoplacental capillary elaboration relative to CD1 mice, a prolific outbred strain. Such strain differences suggest that genetics is an important factor in labyrinthine capillarization.

Relative to CD1 placentas, capillary growth was blunted in B6 placentas in late gestation despite having higher HIF-1α and VEGF protein levels. We found that total tissue HIF-1α as measured by Western blot analysis was increased and that immunohistochemical images showed an apparent elevation in HIF-1α protein in the cytoplasm of B6 placentas. It is possible that HIF-1α was not elevated in the nucleus, where HIF-1α exerts its transcription factor activity, as nuclear expression was difficult to discern. HIF-2α, which is also known to be important in human placentation (46), was not examined. It is possible that the apparent paradox of high VEGF protein and blunted capillary growth may be explained by the existence of

Table 4. *Measurements of the fetoplacental arterial tree as measured by micro-CT*

	CD1 Mice			B6 Mice		
	E13.5	E15.5	E17.5	E13.5	E15.5	E17.5
No. of placentas/group	8	9	8	7	10	8
Vascular volume, mm^3	1.51 ± 0.09[a]	2.08 ± 0.16[b]	2.41 ± 0.19[b]	1.73 ± 0.08[a]	2.14 ± 0.07[b]	2.74 ± 0.16[c]
Vascular depth, mm	0.92 ± 0.03[a]	1.15 ± 0.02[b]	1.30 ± 0.04[b]	0.86 ± 0.04[a]	1.01 ± 0.04[a,*]	1.32 ± 0.04[b]
Vascular span, mm	6.27 ± 0.10	6.58 ± 0.11	6.48 ± 0.07	6.44 ± 0.07	6.25 ± 0.07	6.66 ± 0.05
Umbilical artery diameter, mm	0.32 ± 0.02[a,*]	0.46 ± 0.01[b]	0.54 ± 0.01[c]	0.39 ± 0.02[a]	0.51 ± 0.02[b]	0.50 ± 0.01[b]
No. of vessel segments	1136 ± 111	1117 ± 79	1164 ± 78	1358 ± 52	1368 ± 80	1359 ± 61
Total length of vasculature, mm	261 ± 14[a]	291 ± 15[a]	324 ± 14[b]	278 ± 6[a]	299 ± 8[a]	332 ± 9[a]
Diameter scaling coefficient	−2.82 ± 0.10[a]	−2.77 ± 0.06[a]	−3.04 ± 0.25[a]	−3.03 ± 0.04[a]	−3.05 ± 0.08[a]	−3.51 ± 0.21[b,*]
Length-to-diameter ratio	2.67 ± 0.70	2.82 ± 0.63	2.91 ± 0.82	2.36 ± 0.59	2.32 ± 0.53	2.37 ± 0.65

Data are means ± SE. [a,b,c]Different letters show a significant difference between gestational ages ($P < 0.05$); *$P < 0.05$, significant differences between strains at the same gestational age as determined by two-way ANOVA followed by Tukey post hoc tests.

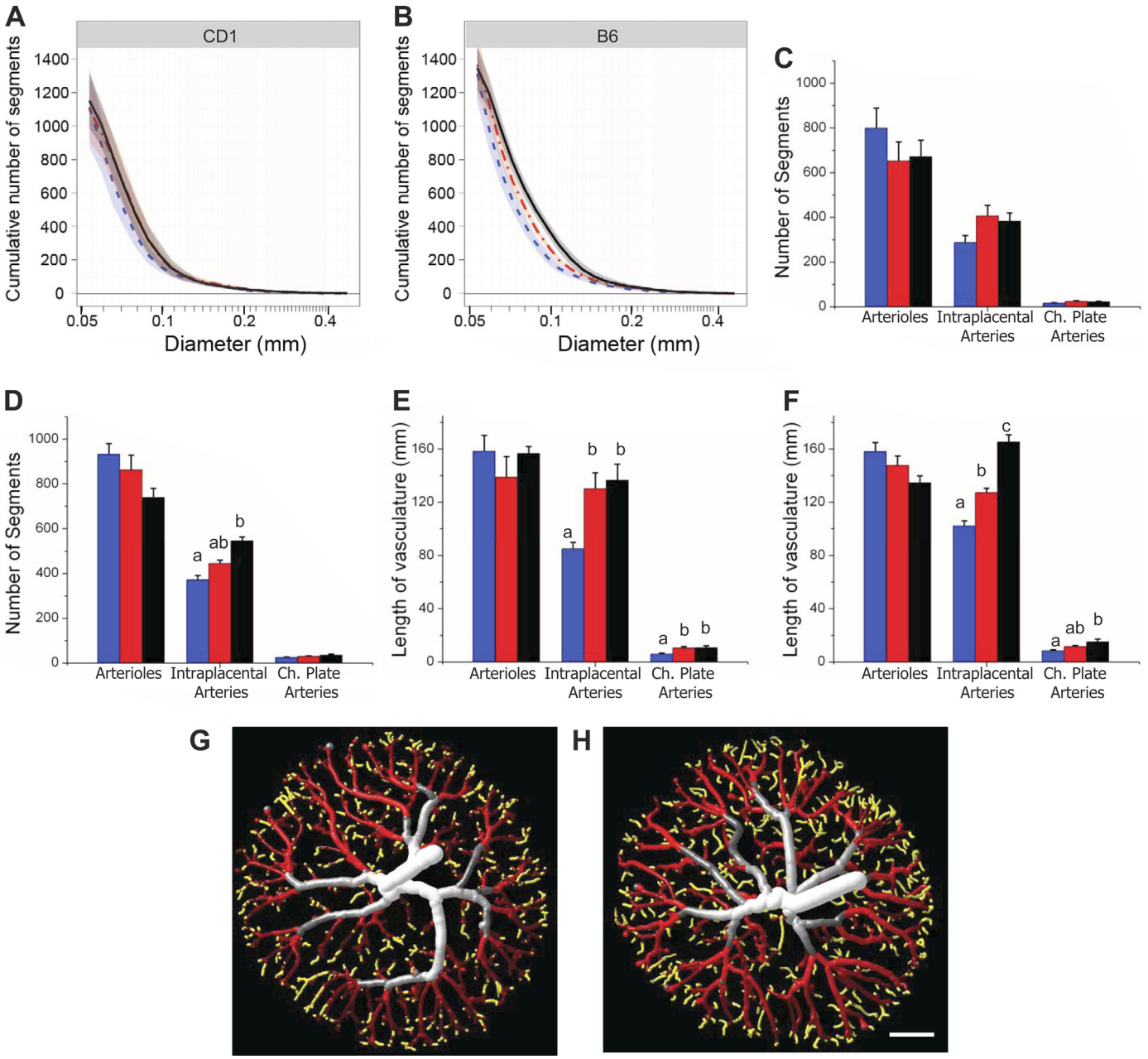

Fig. 6. Distribution of vessel segments. Cumulative distributions of vessel diameters in CD1 (*A*) and B6 (*B*) placentas at E13.5 (blue dotted line), E15.5 (red dashed-dotted line), and E17.5 (black solid line) are shown. Shaded regions represent the 95% confidence interval for each mean curve; n = 7–10 placental specimens/group (including ≥4 dams/group and 1–3 specimens/litter). Note the rightward shift in the curves between E13.5 and E15.5 for both strains primarily in the mid diameter range. A further rightward shift from E15.5 to E17.5 was evident for B6 mice only, whereas the E15.5 and E17.5 curves (red and black lines) were virtually superimposable for CD1 mice. *C* and *D*: numbers of vessel segments within three diameter ranges [arterioles (50–75 μm), intraplacental arteries (75–150 μm), and chorionic (Ch) plate arteries (>200 μm)] for CD1 (*C*) and B6 placentas (*D*) at E13.5 (blue bars), E15.5 (red bars), and E17.5 (black bars). *E* and *F*: total lengths of vessels in those size ranges for CD1 (*E*) and B6 (*F*) placentas. To visualize the location of vessel diameters within the tree, example E15.5 CD1 (*G*) and B6 (*H*) tubular models have been color rendered to depict vessel diameters. Chorionic plate vessels are displayed in gray and white, intraplacental arteries are shown in red, and arterioles are shown in yellow. Scale bar = 1 mm. [a,b,c]Different letters show a significant difference between gestational ages ($P < 0.05$; two-way ANOVA, followed by Tukey post hoc test).

anti-angiogenic VEGF isoforms, which are formed through alternative splicing of exon 8 (6). Because the proximal portion of pro- and antiangiogenic isoforms are identical, and the antibody used was designed to detect the first 140 amino acids of VEGF, it is likely that the antibody detected both pro- and antiangiogenic isoforms. Thus, the blunted capillary growth in B6 mice could be due to higher expression of the antiangiogenic VEGF isoforms. Alternatively, it is also possible that increased expression of proangiogenic VEGF isoforms caused the observed increase in intraplacental arterial diameters but that the adjacent capillaries failed to respond due to reduced angiogenic sensitivity. This would be consistent with prior work (58) showing that the B6 angiogenic response to hypoxia was significantly less than the CD1 response. The augmented

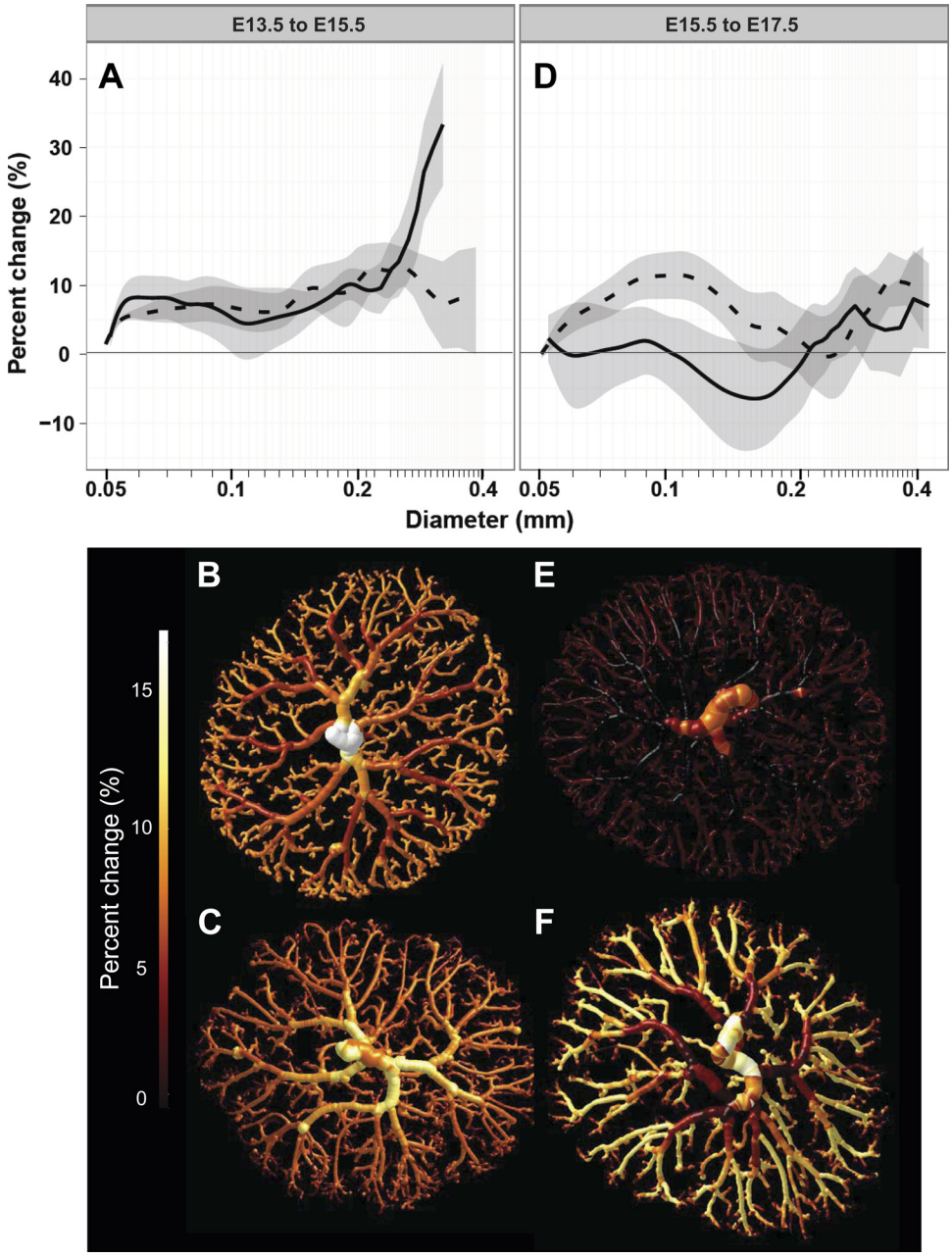

Fig. 7. Growth modeling in CD1 (solid line) and B6 (dashed line) placentas. *A*: percent change in diameter from E13.5 to E15.5 plotted against vessel diameter. ANOVA revealed that the percent change in diameter of the chorionic plate-sized arteries differed significantly between strains. *B* and *C*: iso-surfaces color rendered to show the percent enlargement in an example CD1 (*B*) and B6 (*C*) tree over this time period. *D*: ANOVA revealed that the percent enlargement of the arteriole and intraplacental artery-sized vessels from E15.5 to E17.5 differed between strains. *E* and *F*: iso-surface color renderings showing little to no increase in CD1 trees (*E*) and significant enlargement in B6 trees (*F*). Data are shown as mean ± 95% confidence interval; n = 7–10 placental specimens/group (including ≥4 dams/group and 1–3 specimens/litter).

late gestational enlargement of intraplacental arteries, an apparently blunted angiogenic response by capillaries, elevated labyrinth cell death rates (20), and reduced fetal weight gain relative to CD1 mice all suggest abnormal placental development in late gestation in B6 mice and highlights an important role for genetics.

Developmental changes in the arterial tree. Changes in arterial trees during development have not previously been assessed in any organ, including the placenta. During the maturation phase of the placenta, from E13.5 to E17.5 (near term), fetal weight increased fivefold. Placental gene expression in the maturation phase (>E13.5) markedly differs from that observed during organogenesis (<E13.5) (35). In the maturation phase, labyrinth and capillary volumes substantially increase (12, 14, 15), as confirmed in the present study. We therefore anticipated that the arterial tree would similarly expand by increasing the number of branches, thereby increasing total vessel number to supply the larger capillary bed. Nevertheless, the total number of vessels in both strains stayed constant throughout late gestation. At the E13.5 and 15.5 time points, almost all parameters assessed were statistically identical in CD1 and B6 mice. Although there were no changes in total segment number, vessel diameters increased from E13.5 to 15.5 in both strains. In contrast, from E15.5 to E17.5, diameters ceased to increase in CD1 placentas, whereas intraplacental arteries in B6 placentas continued to enlarge. The growth modeling analysis highlighted that, although 50- to 75-μm arterioles appeared to gradually enlarge into 75- to 150-μm intraplacental arteries throughout late gestation in B6 mice, they were not replaced by the enlargement of even smaller (<50 μm) vessels into the 50- to 75-μm range. This may be explained by the very low number of vessels in the 10- to 50-μm range, as observed from

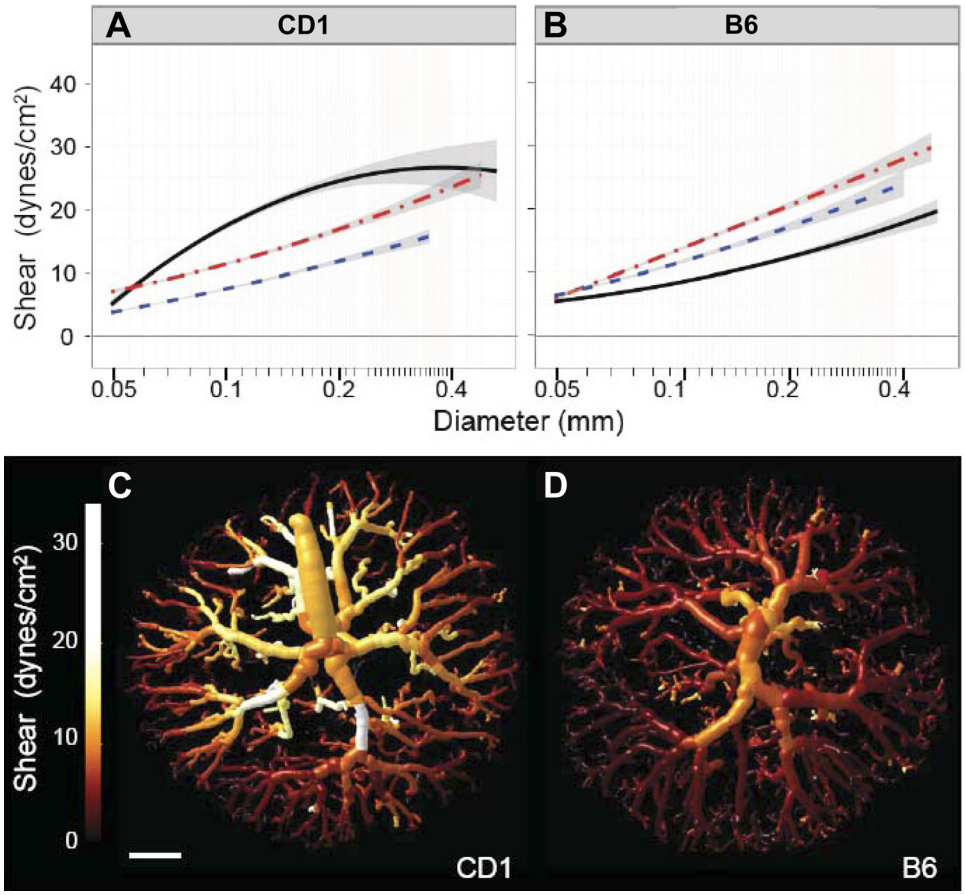

Fig. 8. Shear stress during late gestation. *A* and *B*: distribution of shear in fetoplacental arterial tree CD1 (*A*) and B6 (*B*) placentas at E13.5 (blue dotted line), E15.5 (red dashed-dotted line), and E17.5 (black solid line). Data are shown as mean ± 95% confidence intervals of the mean; n = 7–10 placental specimens/group (including ≥4 dams/group and 1–3 specimens/litter). *C* and *D*: tubular models color rendered to show shear magnitude at E17.5 in example CD1 (*C*) and B6 (*D*) placentas. The CD1 tree demonstrated higher shear throughout. This was most noticeable in the larger vessels, which display more yellow and white coloring compared with the B6 tree. Scale bar = 1 mm.

SEM images. Together, these results suggest that capillaries are not transformed into small arterioles as gestation advances; rather, they may be retained, thereby sustaining or increasing exchange rather than elaborating the arterial tree.

Developmental changes in vascular resistance. Vascular resistance across the placental arterial circulation remained approximately constant through late gestation in CD1 mice but decreased by 50% in B6 mice due to enlargement of vessel diameters within the B6 tree. To calculate resistance, measured vascular geometry and fetal blood viscosity are required. Since no data are available for viscosity fetal mouse blood over this developmental interval, it was necessary to assume the viscosity would be similar to the viscosity of adult blood in small vessels (49). However, fetal red blood cells are larger than adult red blood cells at the gestational ages in this study (33), so viscosity estimates may be low and therefore underestimate resistance. Measurement of fetoplacental arterial vascular resistance is novel; therefore, it is difficult to assess the accuracy of our estimates. Thus, we used pressure and flow values from the literature to calculate total umbilicoplacental resistance and compared those values with our arterial resistance estimates. Literature-based estimates suggested that total placental vascular resistance remains relatively constant across late gestation in CD1 mice and that the resistance estimated for the fetoarterial placental tree from our data accounts for ~1/3 of the total resistance. This proportion is similar to 35% measured as the arterial contribution to total umbilicoplacental vascular resistance in near-term fetal sheep (3). Thus, our arterial resistance calculation appears reasonable. However, constant total and arterial vascular resistance implies that the combined resistance of the capillaries and venous outflow tract also remains unchanged in late gestation. At first this seems surprising because of the large increase in capillary volume. However, if capillary volume increases primarily due to increased length (14), as occurs in human placentas in late gestation (30), this would have relatively little influence on resistance. Any increase in resistance due to an increase in length may be offset by a small increase in the number of capillaries in parallel. Direct measurements of arterial pressure and fetoplacental blood flow in sheep over the last third of gestation found that the increase in flow could be entirely explained by the increase in arterial pressure, whereas the vascular resistance calculated from these data remained constant (25). In summary, our results suggest that arterial resistance remains constant during late gestation in CD1 mice and accounts for ~1/3 of the total resistance across the fetoplacental circulation.

Developmental changes in shear stress. Shear stress increased throughout late gestation in CD1 mice but decreased from E15.5 to E17.5 in B6 mice due to the increased vessel diameters. Shear stress calculations were dependent on flow, diameter, and viscosity and assumed both Poiseuille's Law for flow through a pipe and equal pressure in all terminal vessels. Although differences in shear were observed between strains, the range of shear values we observed within and across specimens was small. This was expected, as wall shear stress is maintained within certain limits during fetal development to maintain homeostasis and prevent vascular anomalies (26). Fetoplacental shear in the mouse has not previously been reported. However, when we calculated aortic shear stress using data for another outbred mouse strain (Swiss

Webster) (47), using the same assumptions for blood viscosity and parabolic laminar flow, we found that it was similar in magnitude and showed a similar twofold increase over 3 gestational days (i.e., 17–35 dyn/cm^2 from E11.5 to 14.5) (48) as we report here for the umbilical artery (~15–30 dyn/cm^2 from E13.5 to E17.5) in outbred CD1 mice. Comparable data for the B6 strain or other inbred strains are not available in the literature. Due to dependence on flow and vessel diameters, shear values differ greatly between species, with an inverse relationship between animal size and wall shear stress (11). Thus, it is not surprising that calculations for humans at term, having a much larger umbilical artery diameter (7) and higher blood velocity (1), yield a much lower umbilical artery shear stress of ~7 dyn/cm^2, threefold lower than ~20 dyn/cm^2 at term in the mouse. Shear is also approximately threefold lower in the mouse common carotid artery compared with that of the human (11). Together, these large variations in shear suggest that wall shear stress is regulated locally, as previously suggested (51). Our data indicate that a constant shear level is not maintained throughout development.

Comparison with the human placenta. The results reported here for the mouse placenta show strong parallels with what is known regarding placental vascular development in humans. In humans, as in CD1 mice, there is a late gestational increase in capillarization (30) and a reduction in interhaemal membrane thickness (10). Additionally, maturation of CD1 trees occurs via elaboration of the capillary bed, rather than by expansion of the arterial tree. This is strikingly similar to the rapid elaboration of terminal villi and capillaries in human placentas after ~22 wk (30). Interestingly, in human IUGR, there is a late gestational blunting of fetal weight gain, reduced placental capillarization, and increased placental cell death rates (22, 36, 39), similar to our observations in B6 mice (20). Elevated VEGF levels were also observed in B6 placentas in the present study. In humans, there is no consistent finding for VEGF levels in IUGR placentas; they can be elevated (5), decreased (38), or unchanged (50). The overall similarities between humans and mice in fetoplacental development highlights the potential utility of mouse models for studying the genetic regulation of placental development and advancing understanding on why it is impaired in pregnancy complications, such as IUGR. In particular, we speculate that B6 mice may model abnormal placental vascularization in human IUGR placentas exhibiting elevated VEGF.

Conclusions. In summary, >60 genes have been implicated in mouse placental morphogenesis and vascularization (for a review, see Ref. 59), but how these genes specifically contribute to vascular branching and tree elaboration in the placenta is largely unknown. In the present study, we observed statistically and physiologically significant differences in vascular development and hemodynamics between two mouse strains, suggesting a prominent role for genetics. The results showed very little expansion of the CD1 arterial tree and constant vascular resistance in late gestation; however, the expansion of intraplacental artery diameters in B6 placentas led to significant decreases in resistance and shear stress. These novel parameters were measurable due to the use of automated vascular segmentation, a technique we have previously shown provides accurate and reproducible measurements of fetoplacental arterial trees (52). Thus, we suggest that the methods described herein will be extremely useful in determining the specific effects of gene expression on arterial tree development and in phenotyping numerous mouse models that currently are suspected to have a placental vascular defect.

GRANTS

This work was funded by Heart and Stroke Foundation of Ontario Grants NA5804 and T6297 and by Canadian Institute of Health Research Grants MOP86734 and MOP93618. M. Y. Rennie was funded by an Ontario Graduate Scholarship. S. L. Adamson gratefully acknowledges support as the Anne and Max Tanenbaum Chair in Molecular Medicine at Mount Sinai Hospital.

DISCLOSURES

No conflicts of interest, financial or otherwise, are declared by the author(s).

AUTHOR CONTRIBUTIONS

Author contributions: M.Y.R., J.D., S.L.A., and J.G.S. conception and design of research; M.Y.R., J.D., and K.J.W. performed experiments; M.Y.R., J.D., S.L.A., and J.G.S. analyzed data; M.Y.R., S.L.A., and J.G.S. interpreted results of experiments; M.Y.R. prepared figures; M.Y.R., S.L.A., and J.G.S. drafted manuscript; M.Y.R., J.D., K.J.W., A.J., S.L.A., and J.G.S. edited and revised manuscript; M.Y.R., J.D., K.J.W., A.J., S.L.A., and J.G.S. approved final version of manuscript.

REFERENCES

1. **Acharya G, Wilsgaard T, Berntsen GK, Maltau JM, Kiserud T.** Reference ranges for serial measurements of blood velocity and pulsatility index at the intra-abdominal portion, and fetal and placental ends of the umbilical artery. *Ultrasound Obstet Gynecol* 26: 162–169, 2005.
2. **Adamson SL, Lu Y, Whiteley KJ, Holmyard D, Hemberger M, Pfarrer C, Cross JC.** Interactions between trophoblast cells and the maternal and fetal circulation in the mouse placenta. *Dev Biol* 250: 358–373, 2002.
3. **Adamson SL, Morrow RJ, Bull SB, Langille BL.** Vasomotor responses of the umbilical circulation in fetal sheep. *Am J Physiol Regul Integr Comp Physiol* 256: R1056–R1062, 1989.
4. **Anson-Cartwright L, Dawson K, Holmyard D, Fisher SJ, Lazzarini RA, Cross JC.** The glial cells missing-1 protein is essential for branching morphogenesis in the chorioallantoic placenta. *Nat Genet* 25: 311–314, 2000.
5. **Barut F, Barut A, Gun BD, Kandemir NO, Harma MI, Harma M, Aktunc E, Ozdamar SO.** Intrauterine growth restriction and placental angiogenesis. *Diagn Pathol* 5: 24, 2010.
6. **Bates DO, Cui TG, Doughty JM, Winkler M, Sugiono M, Shields JD, Peat D, Gillatt D, Harper SJ.** VEGF165b, an inhibitory splice variant of vascular endothelial growth factor, is down-regulated in renal cell carcinoma. *Cancer Res* 62: 4123–4131, 2002.
7. **Benirschke K, Kaufmann P, Baergen RN.** *Pathology of the Human Placenta.* New York: Springer, 2006.
8. **Bridgewater D, Rosenblum ND.** Stimulatory and inhibitory signaling molecules that regulate renal branching morphogenesis. *Pediatr Nephrol* 24: 1611–1619, 2009.
9. **Burton GJ, Feneley MR.** Capillary volume fraction is the principal determinant of villous membrane thickness in the normal human placenta at term. *J Dev Physiol* 17: 39–45, 1992.
10. **Burton GJ, Jauniaux E.** Sonographic, stereological and Doppler flow velocimetric assessments of placental maturity. *Br J Obstet Gynaecol* 102: 818–825, 1995.
11. **Cheng C, Helderman F, Tempel D, Segers D, Hierck B, Poelmann R, van TA, Duncker DJ, Robbers-Visser D, Ursem NT, van HR, Wentzel JJ, Gijsen F, van der Steen AF, de CR, Krams R.** Large variations in absolute wall shear stress levels within one species and between species. *Atherosclerosis* 195: 225–235, 2007.
12. **Coan PM, Angiolini E, Sandovici I, Burton GJ, Constancia M, Fowden AL.** Adaptations in placental nutrient transfer capacity to meet fetal growth demands depend on placental size in mice. *J Physiol* 586: 4567–4576, 2008.
13. **Coan PM, Conroy N, Burton GJ, Ferguson-Smith AC.** Origin and characteristics of glycogen cells in the developing murine placenta. *Dev Dyn* 235: 3280–3294, 2006.
14. **Coan PM, Ferguson-Smith AC, Burton GJ.** Developmental dynamics of the definitive mouse placenta assessed by stereology. *Biol Reprod* 70: 1806–1813, 2004.

15. **Coan PM, Vaughan OR, Sekita Y, Finn SL, Burton GJ, Constancia M, Fowden AL.** Adaptations in placental phenotype support fetal growth during undernutrition of pregnant mice. *J Physiol* 588: 527–538, 2010.
16. **Coultas L, Chawengsaksophak K, Rossant J.** Endothelial cells and VEGF in vascular development. *Nature* 438: 937–945, 2005.
17. **Cox B, Kotlyar M, Evangelou AI, Ignatchenko V, Ignatchenko A, Whiteley K, Jurisica I, Adamson SL, Rossant J, Kislinger T.** Comparative systems biology of human and mouse as a tool to guide the modeling of human placental pathology. *Mol Syst Biol* 5: 279, 2009.
18. **Cross JC, Baczyk D, Dobric N, Hemberger M, Hughes M, Simmons DG, Yamamoto H, Kingdom JC.** Genes, development and evolution of the placenta. *Placenta* 24: 123–130, 2003.
19. **Cross JC, Simmons DG, Watson ED.** Chorioallantoic morphogenesis and formation of the placental villous tree. *Ann NY Acad Sci* 995: 84–93, 2003.
20. **Detmar J.** *Regulation of Cell Death During Murine Placental Development and Its Dysregulation Due to Xenobiotic Exposure* (PhD dissertation). Toronto, ON, Canada: University of Toronto, 2007.
21. **Detmar J, Rennie MY, Whiteley KJ, Qu D, Taniuchi Y, Shang X, Casper RF, Adamson SL, Sled JG, Jurisicova A.** Fetal growth restriction triggered by polycyclic aromatic hydrocarbons is associated with altered placental vasculature and AhR-dependent changes in cell death. *Am J Physiol Endocrinol Metab* 295: E519–E530, 2008.
22. **Endo H, Okamoto A, Yamada K, Nikaido T, Tanaka T.** Frequent apoptosis in placental villi from pregnancies complicated with intrauterine growth restriction and without maternal symptoms. *Int J Mol Med* 16: 79–84, 2005.
23. **Georgiades P, Ferguson-Smith AC, Burton GJ.** Comparative developmental anatomy of the murine and human definitive placentae. *Placenta* 23: 3–19, 2002.
24. **Guidolin D, Crivellato E, Ribatti D.** The "self-similarity logic" applied to the development of the vascular system. *Dev Biol* 351: 156–162, 2011.
25. **Hedriana HL, Brace RA, Gilbert WM.** Changes in blood flow to the ovine chorion and amnion across gestation. *J Soc Gynecol Investig* 2: 727–734, 1995.
26. **Hove JR, Koster RW, Forouhar AS, cevedo-Bolton G, Fraser SE, Gharib M.** Intracardiac fluid forces are an essential epigenetic factor for embryonic cardiogenesis. *Nature* 421: 172–177, 2003.
27. **Hsia CC, Hyde DM, Ochs M, Weibel ER.** An official research policy statement of the American Thoracic Society/European Respiratory Society: standards for quantitative assessment of lung structure. *Am J Respir Crit Care Med* 181: 394–418, 2010.
28. **Huang Y, Guo X, Kassab GS.** Axial nonuniformity of geometric and mechanical properties of mouse aorta is increased during postnatal growth. *Am J Physiol Heart Circ Physiol* 290: H657–H664, 2006.
29. **Ishiwata T, Nakazawa M, Pu WT, Tevosian SG, Izumo S.** Developmental changes in ventricular diastolic function correlate with changes in ventricular myoarchitecture in normal mouse embryos. *Circ Res* 93: 857–865, 2003.
30. **Jackson MR, Mayhew TM, Boyd PA.** Quantitative description of the elaboration and maturation of villi from 10 weeks of gestation to term. *Placenta* 13: 357–370, 1992.
31. **Jensen EB, Gundersen HJ, Osterby R.** Determination of membrane thickness distribution from orthogonal intercepts. *J Microsc* 115: 19–33, 1979.
32. **Kassab GS.** Scaling laws of vascular trees: of form and function. *Am J Physiol Heart Circ Physiol* 290: H894–H903, 2006.
33. **Kingsley PD, Malik J, Fantauzzo KA, Palis J.** Yolk sac-derived primitive erythroblasts enucleate during mammalian embryogenesis. *Blood* 104: 19–25, 2004.
34. **Kline TL, Zamir M, Ritman EL.** Relating function to branching geometry: a micro-CT study of the hepatic artery, portal vein, and biliary tree. *Cells Tissues Organs* 194: 431–442, 2011.
35. **Knox K, Baker JC.** Genomic evolution of the placenta using co-option and duplication and divergence. *Genome Res* 18: 695–705, 2008.
36. **Krebs C, Macara LM, Leiser R, Bowman AW, Greer IA, Kingdom JC.** Intrauterine growth restriction with absent end-diastolic flow velocity in the umbilical artery is associated with maldevelopment of the placental terminal villous tree. *Am J Obstet Gynecol* 175: 1534–1542, 1996.
37. **Kulandavelu S.** *Cardiovascular, Utero- and Fetoplacental Function in Mice During Normal Pregnancy and in the Absence of Endothelial Nitric Oxide Synthase* (PhD dissertation). Toronto, Canada: University of Toronto, 2009.
38. **Lyall F, Young A, Boswell F, Kingdom JC, Greer IA.** Placental expression of vascular endothelial growth factor in placentae from pregnancies complicated by pre-eclampsia and intrauterine growth restriction does not support placental hypoxia at delivery. *Placenta* 18: 269–276, 1997.
39. **Macara L, Kingdom JC, Kaufmann P, Kohnen G, Hair J, More IA, Lyall F, Greer IA.** Structural analysis of placental terminal villi from growth-restricted pregnancies with abnormal umbilical artery Doppler waveforms. *Placenta* 17: 37–48, 1996.
40. **Metzger RJ, Klein OD, Martin GR, Krasnow MA.** The branching programme of mouse lung development. *Nature* 453: 745–750, 2008.
41. **Metzger RJ, Krasnow MA.** Genetic control of branching morphogenesis. *Science* 284: 1635–1639, 1999.
42. **Morrisey EE, Hogan BL.** Preparing for the first breath: genetic and cellular mechanisms in lung development. *Dev Cell* 18: 8–23, 2010.
43. **Mu J, Adamson SL.** Developmental changes in hemodynamics of the uterine artery, the utero- and umbilico-placental, and vitelline circulations in the mouse throughout gestation. *Am J Physiol Heart Circ Physiol* 291: H1421–H1428, 2006.
44. **Nordsletten DA, Blackett S, Bentley MD, Ritman EL, Smith NP.** Structural morphology of renal vasculature. *Am J Physiol Heart Circ Physiol* 291: H296–H309, 2006.
45. **Op Den BJ, Bajzer Z, Ritman EL.** Branching morphology of the rat hepatic portal vein tree: a micro-CT study. *Ann Biomed Eng* 34: 1420–1428, 2006.
46. **Patel J, Landers K, Mortimer RH, Richard K.** Regulation of hypoxia inducible factors (HIF) in hypoxia and normoxia during placental development. *Placenta* 31: 951–957, 2010.
47. **Phoon CK, Aristizabal O, Turnbull DH.** 40 MHz Doppler characterization of umbilical and dorsal aortic blood flow in the early mouse embryo. *Ultrasound Med Biol* 26: 1275–1283, 2000.
48. **Phoon CK, Aristizabal O, Turnbull DH.** Spatial velocity profile in mouse embryonic aorta and Doppler-derived volumetric flow: a preliminary model. *Am J Physiol Heart Circ Physiol* 283: H908–H916, 2002.
49. **Pries AR, Secomb TW.** Rheology of the microcirculation. *Clin Hemorheol Microcirc* 29: 143–148, 2003.
50. **Rajakumar A, Jeyabalan A, Markovic N, Ness R, Gilmour C, Conrad KP.** Placental HIF-1α, HIF-2α, membrane and soluble VEGF receptor-1 proteins are not increased in normotensive pregnancies complicated by late-onset intrauterine growth restriction. *Am J Physiol Regul Integr Comp Physiol* 293: R766–R774, 2007.
51. **Reneman RS, Arts T, Hoeks AP.** Wall shear stress–an important determinant of endothelial cell function and structure–in the arterial system in vivo. Discrepancies with theory. *J Vasc Res* 43: 251–269, 2006.
52. **Rennie MY, Detmar J, Whiteley KJ, Yang J, Jurisicova A, Adamson SL, Sled JG.** Vessel tortuousity and reduced vascularization in the fetoplacental arterial tree after maternal exposure to polycyclic aromatic hydrocarbons. *Am J Physiol Heart Circ Physiol* 300: H675–H684, 2011.
53. **Rennie MY, Whiteley KJ, Kulandavelu S, Adamson SL, Sled JG.** 3D visualisation and quantification by microcomputed tomography of late gestational changes in the arterial and venous feto-placental vasculature of the mouse. *Placenta* 28: 833–840, 2007.
54. **Sherman TF.** On connecting large vessels to small. The meaning of Murray's law. *J Gen Physiol* 78: 431–453, 1981.
55. **Sled JG, Marxen M, Henkelman RM.** *Analysis of Micro-Vasculature in Whole Kidney Specimens Using Micro-CT*. Bellingham: Spie-Int Soc Optical Engineering, 2004.
56. **van der WL, Adams DJ, Bradley A.** Tools for targeted manipulation of the mouse genome. *Physiol Genomics* 11: 133–164, 2002.
57. **Veras MM, Damaceno-Rodrigues NR, Caldini EG, Maciel Ribeiro AA, Mayhew TM, Saldiva PH, Dolhnikoff M.** Particulate urban air pollution affects the functional morphology of mouse placenta. *Biol Reprod* 79: 578–584, 2008.
58. **Ward NL, Moore E, Noon K, Spassil N, Keenan E, Ivanco TL, LaManna JC.** Cerebral angiogenic factors, angiogenesis, and physiological response to chronic hypoxia differ among four commonly used mouse strains. *J Appl Physiol* 102: 1927–1935, 2007.
59. **Watson ED, Cross JC.** Development of structures and transport functions in the mouse placenta. *Physiology (Bethesda)* 20: 180–193, 2005.
60. **Whiteley KJ, Pfarrer CD, Adamson SL.** Vascular corrosion casting of the uteroplacental and fetoplacental vasculature in mice. *Methods Mol Med* 121: 371–392, 2006.
61. **Yang J, Yu LX, Rennie MY, Sled JG, Henkelman RM.** Comparative structural and hemodynamic analysis of vascular trees. *Am J Physiol Heart Circ Physiol* 298: H1249–H1259, 2010.